

REFERENCES

1. Cheng AC, Lucas PW, Yuen HK, et al. Surgical anatomy of the Chinese orbit. *Ophthalm Plast Reconstr Surg* 2008;24:136–141
2. Danko I, Haug RH. An experimental investigation of the safe distance for internal orbital dissection. *J Oral Maxillofac Surg* 1998;56:749–752
3. Ji Y, Qian Z, Dong Y, et al. Quantitative morphometry of the orbit in Chinese adults based on a three-dimensional reconstruction method. *J Anat* 2010;217:501–506
4. Lederman IR. Loss of vision associated with surgical treatment of zygomatic-orbital floor fracture. *Plast Reconstr Surg* 1981;68:94–98
5. Ord RA. Post-operative retrobulbar haemorrhage and blindness complicating trauma surgery. *Br J Oral Surg* 1981;19:202–207
6. Holt GR, Holt JE. Incidence of eye injuries in facial fractures: an analysis of 727 cases. *Otolaryngol Head Neck Surg* 1983;91:276–279
7. Kline LB, Morawetz RB, Swaid SN. Indirect injury of the optic nerve. *Neurosurgery* 1984;14:756–764
8. Stankiewicz JA. Blindness and intranasal endoscopic ethmoidectomy: prevention and management. *Otolaryngol Head Neck Surg* 1989;101:320–329
9. Hayek G, Mercier P, Fournier H. Anatomy of the orbit and its surgical approach. *Advances and Technical Standards in Neurosurgery*. Berlin: Springer; 2006
10. McQueen CT, Diruggiero DC, Campbell JP, et al. Orbital osteology: a study of the surgical landmarks. *Laryngoscope* 1995;105:783–788
11. Rontal E, Rontal M, Guilford F. Surgical anatomy of the orbit. *Ann Otol Rhinol Laryngol* 1978;88:382–386
12. Sullivan L, Romney CP. Cleaning and preserving animal skulls. Tucson, AZ: The University of Arizona Cooperative Extension, College of Agriculture; 1999. Available at: <http://extension.arizona.edu/sites/extension.arizona.edu/files/pubs/az1144.pdf>. Accessed September 6, 2016
13. Hwang K, Baik SH. Surgical anatomy of the orbit of Korean adults. *J Craniofac Surg* 1999;10:129–134
14. Karakaş P, Bozkir M, Oguz Ö. Morphometric measurements from various reference points in the orbit of male Caucasians. *Surg Radiol Anat* 2002;24:358–362
15. Munguti J, Mandela P, Butt F. Referencing orbital measures for surgical and cosmetic procedures. *Ant J of Africa* 2012;1:40–45
16. Huanmanop M, Sithiporn Agthong M, Vilai Chentanez M. Surgical anatomy of fissures and foramina in the orbits of Thai adults. *J Med Assoc Thai* 2007;90:2383–2391
17. Fetouh FA, Mandour D. Morphometric analysis of the orbit in adult Egyptian skulls and its surgical relevance. *Eur J Anat* 2014;18:303–315
18. Oladipo G, Olotu J, Suleiman Y. Anthropometric studies of cephalic indices of the Ogonis in Nigeria. *Asian J Med Sci* 2009;1:15–17
19. Dutton JJGG, Wiseman JB, Holck DE. Evaluation and treatment of orbital fractures. A multidisciplinary approach. *Anatomy, Radiology, and Patient Evaluation*. Philadelphia, PA: Elsevier Saunders; 2006
20. Kirchner JA, Yanagisawa E, Crelin ESJR. Surgical anatomy of the ethmoidal arteries. A laboratory study of 150 orbits. *Arch Otolaryngol* 1961;74:382–386

beam computed tomography (CBCT) in different planes of section (coronal and sagittal).

Materials and Methods: CBCT images of 177 subjects of which 51 males and 126 females in the age group of 11 to 73 years were included in the study population. Linear dimensions which include the length, depth, diameter, and interclinoid distance were measured and the shape of sella turcica was analyzed.

Results: Sella turcica had circular morphology in 69.5% of the subjects while flattened shape of sella turcica was observed in 16.4%, oval shape of sella turcica in 14%. There was no significant difference in the all measurements of sella turcica between males and females ($P > 0.05$). Diameter ($P < 0.01$), depth ($P < 0.001$), length ($P < 0.05$), and interclinoid distance ($P < 0.05$) of the sella turcica differed significantly with age.

Conclusions: The anatomical structure of sella turcica can be studied effectively in CBCT images. Linear dimensions and shape of sella turcica in the current study can be used as reference standards for further investigations.

Key Words: Anterior clinoid process, cone beam computed tomography, cone beam CT, morphology, pituitary, sella turcica

The pituitary gland can be defined as the primary gland of the body since it controls the majority of endocrine functions. It is housed in the sella turcica and is located in close proximity to numerous vital structures such as the sphenoid sinus, optic chiasm, cavernous sinus, and hypothalamus. The development of the sella turcica is closely related to that of the pituitary gland.¹ The functional matrix theory states that “the origin, development, and maintenance of all skeletal units are secondary, compensatory, and mechanically obligatory responses to temporally and operationally prior demands of related functional matrices.”² Based on this theory, it can be hypothesized that the pituitary gland serves as the functional matrix of the sella turcica. Literature reports have revealed that whenever the size of the pituitary gland changes, there is a corresponding change in the size of the sella turcica.^{3–7} Radiological assessment of enlarged or abnormally small sella turcica is associated with pathological conditions or hypofunction of the pituitary gland.^{8–13} Deviations in the pituitary gland and in the sella turcica are presumed to be interrelated, and understanding the anatomy and dimensions of the sella turcica is essential to understanding its normal appearance. Moreover, evaluation of the sella turcica is an imperative part of the assessment and diagnosis of the broad spectrum of pathology involved with the pituitary gland. Although there are morphological differences in every individual,

Morphometric Analysis of Sella Turcica Using Cone Beam Computed Tomography

Yasin Yasa, DDS, PhD,* Ali Ocak, DDS, PhD,†
Ibrahim Sevki Bayraktar, DDS, PhD,‡
Suayip Burak Duman, DDS, PhD,§
and Ismail Gumussoy, DDS, PhD||

Objective: The purpose of this study was to assess morphological shape and morphometric analysis of the sella turcica using cone

From the *Department of Maxillofacial Radiology, Faculty of Dentistry, Ordu University, Ordu; †Department of Maxillofacial Radiology, Faculty of Dentistry, Ataturk University, Erzurum; ‡Department of Maxillofacial Radiology, Faculty of Dentistry, Eskişehir Osmangazi University, Eskişehir; §Department of Maxillofacial Radiology, Faculty of Dentistry, İnönü University, Malatya; and ||Department of Maxillofacial Radiology, Faculty of Dentistry, Recep Tayyip Erdoğan University, Rize, Turkey.

Received August 4, 2016.

Accepted for publication August 27, 2016.

Address correspondence and reprint requests to Dr Yasin Yasa, DDS, PhD, Department of Maxillofacial Radiology, Faculty of Dentistry, Ordu University, Ordu, Turkey; E-mail: yasayasin@yahoo.com

The authors report no conflicts of interest.

Copyright © 2016 by Mutaz B. Habal, MD

ISSN: 1049-2275

DOI: 10.1097/SCS.00000000000003223

the establishment of “norms” helps in the elimination of any abnormalities in such a critical region.

Advanced diagnostic imaging methods have made it possible to perform research that defines the morphology of the sella turcica. Computed tomography (CT) and magnetic resonance imaging (MRI) are widely applied as alternatives to plain radiography with respect to studying and characterizing normal anatomy, since conventional radiography is not sufficient as a result of the superimposition of different craniofacial structures and magnification issues.^{3,14–16} Computed tomography becomes necessary when supportive information concerning bony structures or calcifications is required and is frequently used in imaging of the sella turcica.¹⁷ Conversely, cone beam computed tomography (CBCT) is a more reliable method for evaluating bony structures¹⁸; however, CT involves high cost and radiation exposure. CBCT is often recommended as a dose-sparing technique for maxillofacial imaging.^{19–21} In the current study, we used CBCT to image the sella turcica. This approach allowed us to evaluate the structures without angular or dimensional distortion or superposition and involved lower doses of radiation as compared with conventional radiography and CT.

The purpose of the current study was to assess the morphological shape and morphometric analysis of the sella turcica using CBCT in different planes of section (coronal and sagittal).

MATERIALS AND METHODS

Subjects

A total of 177 subjects (126 females and 51 males, with an age range of 11–73 years) who underwent CBCT examination at Ataturk University for any indication were included in the current study. Individuals with a cleft lip palate, a history of surgery to the hypophyseal area, or symptoms of brain abnormalities referable to the pituitary gland were excluded.

Imaging Procedures

CBCT imaging was conducted using a NewTom 3G (Quantitative Radiology, Verona, Italy) device. The maximum output of the scanner was 110 kV, 15 mAs, and a 0.16-mm voxel size, and the standard exposure time was 5.4 seconds. For imaging, the subject was positioned in a seated posture with the head held upright and the eyes focused on a point straight ahead. The x-ray tube-detector system performed a 360° rotation around the head of the patient, with a scanning time of 36 seconds.

One of the axial views of the dorsum sella was selected as a reference view. Subsequently, 1-mm sagittal slices, made from each corresponding slice of the midsagittal plane, were selected for measurements of depth diameter, length, and shape of the sella turcica. The 1-mm coronal slices, on which the tips of the anterior clinoid processes were observed, were selected for measurements of the interclinoid distance (Fig. 1).

Measurements

The measurements of the sella turcica were performed on the slices defined above. The distances used in the current study were as follows (Fig. 1):

Length: The distance from the tip of the dorsum sella to the tuberculum sella.

Depth: A perpendicular line extending to the deepest point of the sellar floor.

Diameter: The furthest point on the posteroinferior aspect of the hypophyseal fossa to the most superior point on the tuberculum sella.

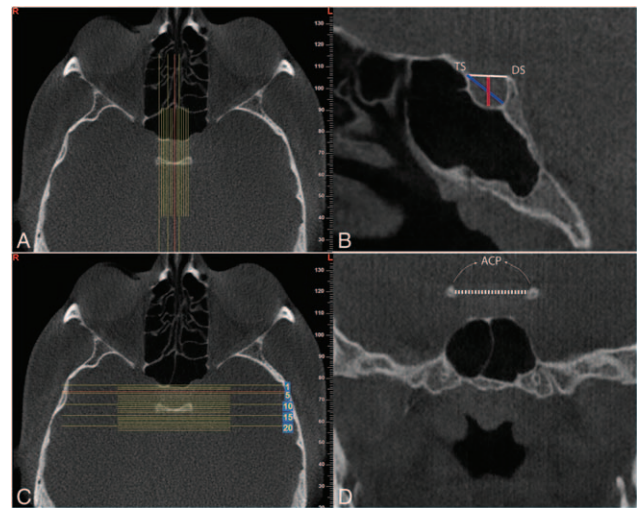


FIGURE 1. (A) Red line showed the midsagittal slice selected as reference view for measurement of length, diameter, and depth. (B) Normal sella turcica morphology and reference lines used for measuring sella turcica size on midsagittal slice: TS, tuberculum sella; DS, dorsum sella; white line, length of sella; blue line, diameter of sella; red line, and depth of sella. (C) Red line showed the coronal slice selected as reference view for measurement of interclinoid distance. (D) ACP, tips of anterior clinoid processes; dashed line, interclinoid distance between ACP.

Interclinoid distance: The distance between the tips of the anterior clinoid processes.

It was described as basic shapes (oval, round, and flattened) according to the sellar floor on the midsagittal images (Fig. 2).

A single examiner performed all measurements. The intra-examiner reliability was assessed for all variables using the intraclass correlation coefficient, and the intraclass correlation coefficients were between 0.85 and 0.96.

SPSS version 20.0 for Windows (SPSS Inc, Chicago, IL) was used for all statistical analysis. Kolmogorov–Smirnov statistics were used for the normality test. An independent *t*-test was used to evaluate differences in sella turcica measurements between genders. One-way analysis of variance and post hoc Tukey test were applied to compare the sella turcica size measurements among different age groups.

RESULTS

The mean dimensions of the sella turcica in subjects according to gender are shown in Table 1. Independent sample *t*-tests comparing the measurements of the sella turcica between genders showed no significant difference ($P > 0.05$). The frequency distribution of dissimilar shapes of the sella turcica among genders is indicated in Table 2. No difference was recorded between genders ($P > 0.05$).

Stratification of the study group was performed according to the age of the subjects. Diameter ($P = 0.003$), depth ($P \leq 0.001$), length

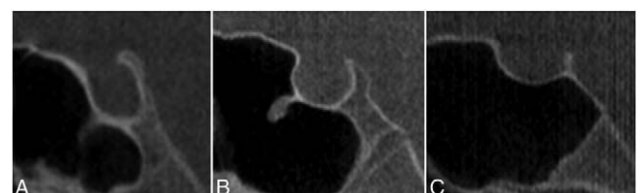


FIGURE 2. Examples of sella shapes: (A) oval; (B) round; and (C) flattened.

TABLE 1. Mean Dimensions of Sella Turcica in the Subjects According to Gender

	Female (n = 126), Mean (SD)	Male (n = 51), Mean (SD)	Total, Mean (SD)	P
Diameter	11.94 (1.58)	11.69 (1.76)	11.87 (1.66)	0.356
Depth	7.96 (1.37)	8.06 (1.24)	7.99 (1.33)	0.667
Length	10.36 (1.75)	10.23 (1.86)	10.32 (1.75)	0.673
Interclinoid distance	18.88 (2.74)	19.74 (2.69)	19.12 (2.74)	0.059

Independent sample *t* test.
n, number of joints; SD, standard deviation.

TABLE 2. Frequency Distribution of Different Shapes of Sella Turcica Among Genders

	Male, n (%)	Female, n (%)	Total, n (%)	χ^2
Oval	8 (4.5)	17 (9.6)	25 (14.1)	0.800
Round	36 (20.3)	87 (49.2)	123 (69.5)	
Flattened	7 (4)	22 (12.4)	29 (16.4)	
Total	51 (28.8)	126 (71.2)	177 (100)	

Chi-squared test.
n, number of subjects.

(*P* = 0.017), and interclinoid distance (*P* = 0.039) of the sella turcica differed significantly with age (Table 3). Measurements of the sella turcica were highest in the group age >45 years and lowest in group age <15 years.

DISCUSSION

A decrease or increase in the function of the functional matrix has an impact on the corresponding skeletal unit. The pituitary gland begins to develop before the formation of the surrounding sella turcica. Certain pathological patients related to hypo/hyperthyroidism have shown that variations in the size of the gland are reflected in the shape and size of the sella turcica. This relationship implies the existence of at least mechanical coordination in the growth of the pituitary gland alongside its enclosing skeletal compartment.^{2,11}

At the time of this writing, dimensional evaluation of the sella turcica is mostly performed with conventional methods such as cephalometric radiography and cadaver studies; however, these also make use of 3-dimensional imaging. Recently, CBCT for dental and maxillofacial diagnostic osseous tasks has been adopted as an alternative to conventional CT. CBCT technology produces images of similar quality to those taken using CT. However, the images are obtained with less expensive equipment and components, a reduced patient examination time and a significantly lower radiation dose

compared with conventional CT. Moreover, the patient scanning procedure and the image reconstruction software connected to CBCT are very user-friendly.^{22,23}

To understand the shape of the sella turcica, the authors have developed several methods. Their classifications were made on the basis of the contours of the sellar floor and the angles of the contours of the anterior and posterior clinoid processes and the tuberculum sellae.^{6,24,25} However, with these subjective classifications made on cephalometric radiographs, it can be difficult to differentiate normal from pathological alterations in the sella turcica related to size. Ruiz et al²⁶ examined the sella turcica in adult human skulls using CT and classified the shapes as U, J, and shallow. The U shape was found in 48% of patients, the J shape in 41%, and the shallow shape in 11%. In the current study, we used basic shapes (oval, circular, and flat) to classify the sella turcica and found that the most frequent shape was circular.

The size of the sella turcica assessed from cephalometric radiographs typically ranges from 4 to 12 mm in height and from 5 to 16 mm in length.^{24,25,27–29} The discrepancies among studies may be due to different landmarks representing the same dimensions, varying degrees of magnification, different compositions of study groups, and superimposition of overlying structures. Quakinine and Hardy³⁰ measured the sella turcica dimensions in a set of 250 sphenoidal blocks from deceased donors, showing that the average width was 12 mm, the average length (anteroposterior diameter) was 8 mm, and the average height (vertical diameter) was 6 mm. The same authors stated that the height of the sella turcica was 2 mm shorter than the width, inferring that the pituitary gland does not fill the entire volume of the sella turcica. Sahni et al, performed a study⁷ using midsagittal MRI sections of the head and autopsies, revealing that the average measurements of the pituitary gland were 11.5 mm in length and 7.4 mm in depth in males and 11.3 mm in length and 7.8 mm in depth in females. They found that the MRI measurements were approximately 1 mm larger than the measurements seen in the autopsies. Ruiz et al²⁶ found that the height of the sella turcica was 6.33 mm and the length was 10.31 mm. In the current study, we had similar results to Ruiz et al, with respect to the height and length measurements. We found that the length of the sella turcica was 10.30 mm and the depth was 7.99 mm. Because Ruiz et al measured the height of the sella turcica using a perpendicular line between the tubercle and the dorsum, this may be the reason why there is a difference in the depth of the sella turcica.

Anatomical knowledge of the anterior and posterior clinoid processes is essential during neurosurgical operations in order to avoid any damage to structures in relation to the pituitary. There are a few studies that have measured the distances between the anterior clinoid processes. Inoue et al,³¹ in their 50 cadaver study, measured the distances between the anterior clinoid tips and found a mean distance of 17.4 mm, with a range from 13.0 to 22.5 mm. Cheng et al³² measured the distance between the apex of the anterior clinoid processes and the sagittal midline in the axial plane on CT

TABLE 3. All Measurements of the Sella Turcica According to Age Groups

	<15, Mean (SD)	15–25, Mean (SD)	25–35, Mean (SD)	35–45, Mean (SD)	>45, Mean (SD)	P
Diameter	11.42 (1.64)	11.55 (1.59)	12.08 (1.69)	12.35 (1.42)	12.85 (1.70)	0.003**
Depth	6.99 (0.91)	7.77 (1.21)	8.36 (1.38)	8.61 (0.93)	8.67 (1.64)	0.0001***
Length	10.36 (2.06)	10.06 (1.64)	10.21 (1.74)	10.39 (1.46)	11.36 (1.90)	0.017*
Interclinoid distance	18.22 (3.25)	18.74 (2.47)	19.89 (2.92)	19.37 (2.96)	20.27 (2.89)	0.039*

One-way analysis of variance.
SD, standard deviation.
P* < 0.05, *P* < 0.01, ****P* < 0.001.

Downloaded from http://journals.lww.com/jcraniofacialsurgery by BhdMfsePfkav1ZEoum1tQIN4a+kLlHEZgbsl on 03/30/2023

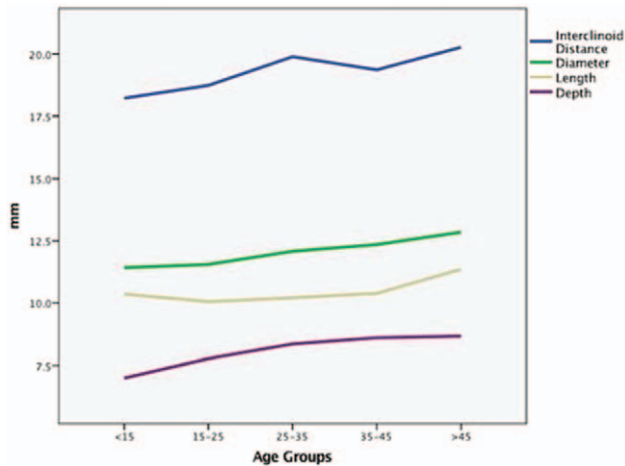


FIGURE 3. Distribution of the length, the depth, the diameter, and the interclinoid distance of the sella turcica according to age groups.

images and found that the anterior clinoid tip was located 12.16 mm from the sagittal midline to the right and 12.48 mm to the left. In the current study, we measured the mean distance between the tips of the anterior clinoid processes on coronal images, and our results were compatible with these findings (Fig. 3).

When linear dimensions were compared with respect to age, the age-related increase in the size of the sella turcica correlated with an increase in the size of the pituitary gland.^{33–35} Indeed, the longitudinal data on the dimensions of the sella turcica imply an increase in size with time, as well as remodeling in the anterior and posterior walls of the cavity.³⁶ Choi et al²⁵ reported that the length, height, and width of the sella turcica increase in a slow but linear manner up to 25 years of age, and in particular, the increase in length was proportional to age. Argyropoulou et al,³³ through their retrospective MRI study, stated that an age-related increase in the size of the sella turcica was probable, since its contents (hypophysitis) were shown to increase with age. Silverman,³⁷ Alkofide,³⁸ and Axelsson⁵ have also mentioned an age-related increase in the size of the sella turcica. We had similar results to the literature and found a steady increase in all dimensions of the sella turcica with age.

Lurie et al³⁹ measured the length, width, and height of the pituitary gland in 35 (16 males and 19 females) adult volunteers by MRI and observed that there was no statistically significant difference in the size of the pituitary gland between the genders. Sakran et al¹³ found no significant difference between males and females concerning the linear dimensions of the sella turcica (length, width, and anteroposterior diameter) in their cadaver study. Alkofide³⁸ performed a study on the lateral cephalograms of 180 individuals and found no significant difference in the linear dimensions between genders. The current study was in accordance with these studies.

CONCLUSIONS

1. The anatomical structure of the sella turcica can be studied effectively in CBCT images. It may be a novel tool for the anatomical analysis of the sella turcica compared with the cadaver, skull study, and CT.
2. In the current study, the linear dimensions and shape of the sella turcica are applicable as reference standards for further investigation in the Turkish population and can also be used to approximate the size of the pituitary gland.

REFERENCES

1. Kjær I. Sella turcica morphology and the pituitary gland—a new contribution to craniofacial diagnostics based on histology and neuroradiology. *Eur J Orthod* 2015;37:28–36
2. Moss ML. The functional matrix hypothesis revisited. 1. The role of mechanotransduction. *Am J Orthod Dentofacial Orthop* 1997;112:8–11
3. Swallow CE, Osborn AG. Imaging of sella and parasellar disease. *Semin Ultrasound CT MRI* 1998;19:257–271
4. Alkofide EA. Sella turcica morphology and dimensions in cleft subjects. *Cleft Palate Craniofac J* 2008;45:647–653
5. Axelsson S, Storhaug K, Kjær I. Post-natal size and morphology of the sella turcica. Longitudinal cephalometric standards for Norwegians between 6 and 21 years of age. *Eur J Orthod* 2004;26:597–604
6. Becktor JP, Einersen S, Kjær I. A sella turcica bridge in subjects with severe craniofacial deviations. *Eur J Orthod* 2000;22:69–74
7. Sahni D, Jit I, Harjeet, et al. Weight and dimensions of the pituitary in northwestern Indians. *Pituitary* 2006;9:19–26
8. Axelsson S, Storhaug K, Kjær I. Post-natal size and morphology of the sella turcica in Williams syndrome. *Eur J Orthod* 2004;26:613–621
9. Bonneville JF, Cattin F, Dietemann JL. Hypothalamic-pituitary region: computed tomography imaging. *Baillieres Clin Endocrinol Metab* 1989;3:35–71
10. Canigur Baybek N, Dincer M. Dimensions and morphologic variations of sella turcica in type 1 diabetic patients. *Am J Orthod Dentofac Orthop* 2014;145:179–187
11. Gopalakrishnan U, Mahendra L, Rangarajan S, et al. The enigma behind pituitary and sella turcica. *Case Rep Dent* 2015;2015:954347
12. Korayem M, Alkofide E. Size and shape of the sella turcica in subjects with Down syndrome. *Orthod Craniofac Res* 2015;18:43–50
13. Sakran AMEA, Khan MA, Altaf FMN, et al. A morphometric study of the sella turcica; gender effect. *Int J Anat Res* 2015;3:927–934
14. Elster AD. Modern imaging of the pituitary. *Radiology* 1993;187:1–14
15. Rennert J, Doerfler A. Imaging of sellar and parasellar lesions. *Clin Neurol Neurosurg* 2007;109:111–124
16. Mazumdar A. Imaging of the pituitary and sella turcica. *Expert Rev Anticancer Ther* 2006;9:S15–S22
17. Tekiner H, Acer N, Kelestimur F. Sella turcica: an anatomical, endocrinological, and historical perspective. *Pituitary* 2015;18:575–578
18. De Vos W, Casselman J, Swennen GRJ. Cone-beam computerized tomography (CBCT) imaging of the oral and maxillofacial region: a systematic review of the literature. *Int J Oral Maxillofac Surg* 2009;38:609–625
19. Ludlow JB, Ivanovic M. Comparative dosimetry of dental CBCT devices and 64-slice CT for oral and maxillofacial radiology. *Oral Surg Oral Med Oral Pathol Oral Radiol Endod* 2008;106:106–114
20. Liang X, Jacobs R, Hassan B, et al. A comparative evaluation of cone beam computed tomography (CBCT) and multi-slice CT (MSCT) part I. On subjective image quality. *Eur J Radiol* 2010;75:265–269
21. Li G. Patient radiation dose and protection from cone-beam computed tomography. *Imaging Sci Dent* 2013;43:63–69
22. Cohnen M, Kemper J, Möbes O, et al. Radiation dose in dental radiology. *Eur Radiol* 2002;12:634–637
23. Schulze D, Heiland M, Thurmann H, et al. Radiation exposure during midfacial imaging using 4- and 16-slice computed tomography, cone beam computed tomography systems and conventional radiography. *Dentomaxillofac Radiol* 2004;33:83–86
24. Sathyanarayana HP, Kailasam V, Chitharanjan AB. Sella turcica—its importance in orthodontics and craniofacial morphology. *Dent Res J (Isfahan)* 2013;10:571–575
25. Choi WJ, Hwang EH, Lee SR. The study of shape and size of normal sella turcica in cephalometric radiographs. *Korean J Oral Maxillofac Radiol* 2001;31:43–49
26. Ruiz CR, Wafae N, Wafae GC. Sella turcica morphometry using computed tomography. *Eur J Anat* 2008;12:47–50
27. Kucia A, Jankowski T, Siewniak M, et al. Sella turcica anomalies on lateral cephalometric radiographs of Polish children. *Dentomaxillofac Radiol* 2014;43:20140165
28. Andredaki M, Koumantanou A, Dorotheou D, et al. A cephalometric morphometric study of the sella turcica. *Eur J Orthod* 2007;29:449–456
29. Nagaraj T, Shruthi R, James L, et al. The size and morphology of sella turcica: a lateral cephalometric study. *J Med Radiol Pathol Surg* 2015;1:3–7

30. Ouaknine GE, Hardy J. Microsurgical anatomy of the pituitary gland and the sellar region. 2. The bony structures. *Am Surg* 1987;53:291–297

31. Inoue A, Ohnishi T, Kohno S, et al. Utility of three-dimensional computed tomography for anatomical assistance in endoscopic endonasal transphenoidal surgery. *Neurosurg Rev* 2015;38:559–565

32. Cheng Y, Wang C, Yang F, et al. Anterior clinoid process and the surrounding structures. *J Craniofac Surg* 2013;24:2098–2102

33. Argyropoulou M, Perignon F, Brunelle F, et al. Height of normal pituitary gland as a function of age evaluated by magnetic resonance imaging in children. *Pediatr Radiol* 1991;21:247–249

34. Sari S, Sari E, Akgun V, et al. Measures of pituitary gland and stalk: from neonate to adolescence. *J Pediatr Endocrinol Metab* 2014;27:1071–1076

35. Chauhan P, Kalra S, Mongia S, et al. Morphometric analysis of sella turcica in North Indian population: a radiological study. *Int J Res Med Sci* 2014;2:521

36. Latham RA. The sella point and postnatal growth of the human cranial base. *Am J Orthod* 1972;61:156–162

37. Silverman FN. Roentgen standards fo-size of the pituitary fossa from infancy through adolescence. *Am J Roentgenol Radium Ther Nucl Med* 1957;78:451–460

38. Alkofide EA. The shape and size of the sella turcica in skeletal Class I, Class II, and Class III Saudi subjects. *Eur J Orthod* 2007;29:457–463

39. Lurie SN, Doraiswamy PM, Husain MM, et al. In vivo assessment of pituitary gland volume with magnetic resonance imaging: the effect of age. *J Clin Endocrinol Metab* 1990;71:505–508

Carotid Artery Aneurysm: A Rare Cause of Hemotympanum

Selçuk Güneş, MD,* Zahide Mine Yazıcı*
 Hakan Selçuk†, Baver Masallah Şimşek, MD,*
 Mustafa Çelik, MD,* and Fatma Tülin Kayhan, MD*

Abstract: Temporal bone fractures can occur as a result of various head trauma. The most common cause of the hemotympanum is traumatic temporal bone fracture. Facial paralysis and hearing loss can be seen associated with temporal bone fracture. The development of the internal carotid artery aneurysm after temporal bone fracture is extremely rare. In this article, the authors evaluated carotid artery aneurysm that developed after temporal fracture and aneurism compressed by coagulated blood mass which showed itself as a hemotympanum. The internal carotid artery aneurysm that induced by temporal bone fracture and presented as hemotympanum has not been reported yet. This patient is the first case in the literature. Diagnosis, treatment, and follow-up options will be discussed in the light of current literature.

From the *Department of Otorhinolaryngology, Istanbul Bakirköy Dr Sadi Konuk Research and Training Hospital; and †Department of Radiology, Bakirköy Sadi Konuk Research and Education Hospital, Istanbul, Turkey.

Received August 7, 2016.

Accepted for publication August 31, 2016.

Address correspondence and reprint requests to Mustafa Çelik, MD, Department of Otolaryngology, Head and Neck Surgery, Istanbul Bakirköy Dr Sadi Konuk Research and Training Hospital, Tevfik Sağlam Caddesi, No 11, 34147 Bakirköy/Istanbul; E-mail: dr.mcelik@yahoo.com

The authors report no conflicts of interest.
 Copyright © 2016 by Mutaz B. Habal, MD
 ISSN: 1049-2275

DOI: 10.1097/SCS.0000000000003237

Key Words: Aneurysm, hemotympanum, internal carotid artery, temporal bone

Internal carotid artery (ICA) aneurysm occurring due to trauma can be extremely mortal. It is usually diagnosed during autopsy. Aneurysm formation is a vascular pathology and the most common etiologies are hypertension, atherosclerosis, and carotid artery dissection.¹ Internal carotid artery aneurysm associated with temporal bone fracture is rarely seen. Hemotympanum is a rare condition typically contingent on a secondary pathology such as temporal bone fracture, chronic middle ear effusion, epistaxis, nasal packing, or coagulation defects. The differential diagnosis of hemotympanum, all potential causes, should be considered. The most common cause of hemotympanum is temporal bone fracture.² The ICA aneurysm that induced by temporal bone fracture and presented as hemotympanum has not been reported yet. This patient is the first case in the literature.

CLINICAL REPORT

A 44-year-old man presented the outpatient clinic with complaint of facial asymmetry and hearing loss that occurred after assaulting. In the otoscopic examination, hemotympanum was detected in the right ear (Fig. 1A). In the right ear, pure tone audiogram revealed conductive hearing loss. Right ear air-bone gap was 35 dB at 0.25 kHz, 35 dB at 0.5 kHz, 35 dB at 1 kHz, 30 dB at 2 kHz, and 25 dB at 4 kHz. At the same frequencies for the left ear was 10, 5, 5, 5, and 4 dB, respectively (Fig. 1B). Tympanometry was type B and acoustic reflex was negative in the right ear. House–Brackmann grade 5 facial paralysis was identified on his right half of face. Other ear, nose, throat, and systemic examination were unremarkable. There was no known history of surgery and systemic disease.

In the temporal bone computed tomography (CT) in the right temporal bone, mixed fracture line and increased density consistent hemotympanum was revealed and there was not any bony dehiscence or bony chain displacement (Fig. 1C).

After initial assessment, decided to medical treatment and follow up. Facial paralysis was decreased with methyl prednisolon treatment. Fourteen days after treatment facial paralysis was at grade 3 according to House–Brackmann scale but conductive type hearing loss and hemotympanum continued despite medical

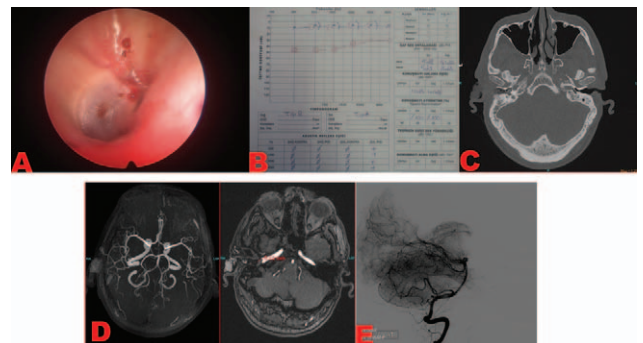


FIGURE 1. (A) Right ear otoscopic image. (B) Pure tone audiogram before treatment. (C) Axial computed tomography image of the temporal bone; mixed fracture line in the right temporal bone. (D) Temporal magnetic resonance angiography images; approximately 4 mm laceration in the lateral wall of petrous segment of the right ICA and saccular pseudoaneurysm. (E) Diagnostic cerebral angiography image: the stent that putted in to petrous segment of the right ICA. Hemotympanum could be a presentation of a serious condition and carotid artery aneurysm should be considered in the differential diagnosis of patients with hemotympanum. ICA, internal carotid artery.